Complex magnetic couplings in Co$_3$TeO$_6$

Chin-Wei Wang,[1] Chi-Hung Lee,[1] Chi-Yen Li,[1] Chun-Ming Wu,[1] Wen-Hsien Li,[1,*] Chih-Chieh Chou,[2] Hung-Duen Yang,[2]
Jeffrey W. Lynn,[3] Qingzhen Huang,[3] A. Brooks Harris,[4] and Helmuth Berger[5]

[1]*Department of Physics and Center for Neutron Beam Applications, National Central University, Jhongli 32001, Taiwan*
[2]*Department of Physics and Center for Nanoscience and Nanotechnology, National Sun Yat-Sen University, Kaohsiung 80424, Taiwan*
[3]*NIST Center for Neutron Research, National Institute of Standards and Technology, Gaithersburg, Maryland 20899, USA*
[4]*Department of Physics and Astronomy, University of Pennsylvania, Philadelphia, Pennsylvania 190104, USA*
[5]*Institute of Physics of Complex Matter, EPFL, Lausanne, Switzerland*

We report powder and single-crystal neutron diffraction measurements, combined with x-ray powder diffraction data, to unravel the complex magnetic phase diagram and exchange coupling in Co$_3$TeO$_6$. The magnetic structures of the various phases differ markedly from those proposed by Ivanov *et al.* [Mater. Res. Bull. **47**, 63 (2012)] on the basis of only powder diffraction data. The dominant exchange interactions are identified by considering the geometrical arrangement of severely distorted CoO$_6$ octahedra and CoO$_4$ tetrahedra, which naturally divide into two different types of layers, one of which consists of zigzag chains. These zigzag chains are the first to develop magnetic order at $T_{M1} = 26$ K, which is incommensurate in nature. The other separate layer of Co spins develops antiferromagnetic order of Γ_4 symmetry at zero wave vector at $T_{M2} = 19.5$ K. Our results are consistent with the previous findings of a spontaneous polarization below $T_{M3} = 18$ K. Our neutron powder diffraction data indicate that the increase in the single-crystal (600) Bragg peak is due to a relief of extinction rather than to magnetic effects associated with the observed anomalous variation in the incommensurate wave vector at $T_{M4} = 16$ K. The commensurate order parameter is shown to have a small dependence on the applied electric field, whereas no such effect is found for the incommensurate ordering. Below T_{M3}, the thermal expansion is negative, and it also exhibits anomalies at T_{M2} and T_{M4}. A symmetry analysis and comprehensive phase diagram are given.

I. INTRODUCTION

Cobalt tellurate Co$_3$TeO$_6$ has been characterized[1–7] as a type-II multiferroic, where the close interplay between the electric and magnetic order parameters generate complex but interesting physical properties of the compound. It is known that materials with magnetoelectric coupling, such as type-II multiferroics,[8–13] are potentially important for spintronics applications.[14] At room temperature, Co$_3$TeO$_6$ has monoclinic symmetry of space group $C2/c$ (No. 15 in Ref. [15]). Several studies[1,4,5] agree that long-range magnetic order sets in below $T_{M1} = 26$ K. However, the nature of the magnetic ordering and the identification of the magnetic phases have been subjects of debate. In the next two sections, we summarize the evidence for our proposed phase diagram. In succeeding sections, we will present (a) thermal expansion data that are consistent with our phase diagram, (b) the dependence of magnetic order on the applied electric field, and (c) the temperature-dependent effects of the relieving of extinction in single-crystal scattering. By considering the structure in terms of severely distorted CoO$_6$ octahedra and CoO$_4$ tetrahedra, we are able to identify the dominant exchange interactions that give rise, respectively, to the commensurate (CM) and incommensurate (ICM) magnetic orders.

II. OVERVIEW OF THE PHASE DIAGRAM

In this section, we describe our view of the phase diagram, which includes results of this and previous papers, mainly Ref. [5]. So far, there exist two quite different proposals for the magnetic structure of Co$_3$TeO$_6$ for temperatures below $T_{M1} = 26$ K. Based on their powder diffraction data,

Ivanov *et al.*[1] concluded that at this temperature CM antiferromagnetic and ICM magnetic orders appear simultaneously. In contrast, our analysis supports the conclusion of Li *et al.*[5] that only ICM order appears at this phase transition into what we call phase A (see Fig. 1). It is extremely unlikely that two different symmetry order parameters should appear at a single continuous phase transition. The data of Li *et al.*[5] give no indication of a first-order transition, although it is impossible to exclude the possibility of a very weak first-order transition. In addition, the analysis of Ivanov *et al.*[1] relies on an analysis of only powder diffraction data. The advantage of the analysis of Li *et al.*[5] is that some of the ICM wave-vector components are fixed by high-quality single-crystal data so that the resulting analysis of the powder diffraction data has fewer adjustable parameters. In fact, from their powder data, Ivanov *et al.*[1] obtain an ICM wave vector in the *b-c* plane, whereas the single-crystal data of Li *et al.*[5] show clearly that both *a* and *b* components of the wave vector are significant. However, in this connection, we also note that one has to be careful not to overinterpret the temperature dependence of the single-crystal Bragg intensities when determining the CM order because these may be subject to corrections due to the relieving of extinction. Therefore, as discussed in detail below, we prefer not to base our interpretations solely on the temperature dependence of the single-crystal CM Bragg intensities but instead rely on powder diffraction data and comparison with the single-crystal data. Here, we focus on phase transitions at zero-applied magnetic field. We remark, though, that a spin-flop transition that affects both the ICM and CM phases appears at magnetic field $B = 9$ T,[5] accompanied by a noticeable reduction in the strength of the electric polarization. Another

ZERO MAGNETIC FIELD

					a, b, c
$P_y \neq 0$	$P_y \neq 0$	$P = 0$	$P = 0$	$P = 0$	**DIEL**
ICM_1	ICM_2	ICM_1	ICM_1	$M(q)=0$	**ICM**
$\Gamma_3 + \Gamma_4$	$\Gamma_3 + \Gamma_4$	Γ_4	$M=0$	$M=0$	**M(q=0)**
5	16	18	19.5	26	
	(T_{M4})	(T_{M3})	(T_{M2})	(T_{M1}) **TEMPERATURE (K)**	
D	**C**	**B**	**A**	**PARA**	**PHASE**
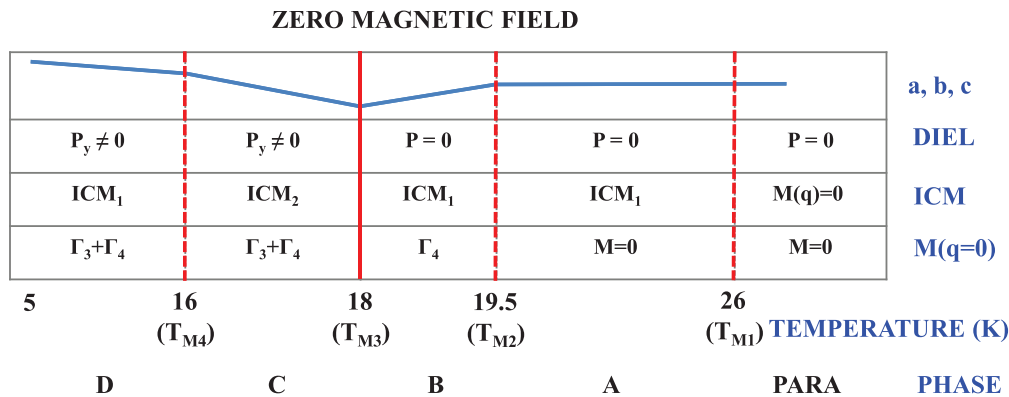
FIG. 1. (Color online) Phase diagram for zero magnetic field, showing the lattice constants (*a, b, c*), the dielectric response, the ICM magnetic order, and the zero wave vector magnetism. The ICM_1 phases have $q = (q_h, q_k, q_l)$ and the ICM_2 phase has $q = (q_h, 0, q_l)$ with $q_h \approx 0.4$, $q_k \approx 0.1$, and $|q_l| \leqslant 0.1$. As shown in the Appendix, the irreps Γ_n can have small admixtures of $\Gamma_{n\pm2}$.

magnetic transition, presumably signifying a second spin-flop transition, has also been observed[4] at $B = 22$ T.

As the temperature is further lowered, the next transition at $T_{M2} = 19.5$ K into phase B is identified from the temperature dependence of the powder diffraction results for the (020) magnetic reflection. As we discuss below, the fact that the powder data for the (600) reflection shows no temperature dependence indicates that the CM magnetic moments are confined to the *ac* plane in contrast to the structure proposed by Ivanov *et al.*[1] in which the moments have nonzero *b* components. If these are ignored, their structure is not very different from what we find here. We agree with Ivanov *et al.*[1] that the CM magnetic structure has the symmetry of the Γ_4 irreducible representation (irrep). However, in contrast with their work, the results of Fig. 3(c) of Li *et al.*[5] clearly indicate that ICM order persists in this phase.

At $T_{M3} = 18$ K, the specific-heat anomaly and the discontinuity in the *k* component of the ICM wave vector found by Li *et al.*,[5] as well as the discontinuity in the second harmonic generation amplitude found by Hudl *et al.*,[3] indicate a first-order phase transition into phase C. The measurements of the spontaneous polarization of Hudl *et al.*[3] indicate "a possible spontaneous polarization ... (close to resolution limit)." Clearer evidence of a spontaneous polarization is provided by Fig. 3 of Tolédano *et al.*[7] Their symmetry analysis of this figure indicates a net ferromagnetic moment $\boldsymbol{M}(0)$ in an arbitrary direction in the *ac* plane and an electric polarization $\boldsymbol{P}$ perpendicular to that plane. This transition can also be inferred from the observation of anomalies in the dielectric constant.[4,5] We should also mention that our single-crystal data categorically excludes having CM order at wave vector $(0, \frac{1}{2}, \frac{1}{4})$ in this phase, as proposed by Ivanov *et al.*[1] Since the magnetic structures assumed by Tolédano *et al.*[7] are incorrect, it is not obvious that their model to explain these phase transitions remains valid.

At $T_{M4} = 16$ K, Fig. 3(c) of Li *et al.*[5] indicates that there is a transition into phase D in which the *k* component of the ICM wave vector (which was zero in phase C) continuously becomes nonzero. Our analysis of our powder diffraction data utilizes the previously determined ICM wave vector to determine the magnetic structures of the octahedral-tetrahedra planes and of the zigzag chains shown below.

As is often found in such multiferroics,[12] our measurements of the temperature dependence of the thermal expansion coefficient show anomalies that correlate nicely with the phase transitions enumerated above. In particular, note that Co_3TeO_6 expands, rather than shrinks, on cooling when an electric polarization develops. If the canonical model of multiferroics[9,10] is maintained, this small spontaneous polarization indicates the presence of two zero wave-vector irreps. Apart from the small spontaneous polarization, the fact that the polarization increases markedly when a magnetic field is applied[3] is reminiscent of the behavior of so-called magnetoelectrics[16] (which are not ferroelectric at zero magnetic field). All these behaviors indicate that the magnetic degrees of freedom are delicately balanced and strongly coupled to the electrical degree of freedom. In this article, we report on the results of studies made on the complex magnetic coupling in Co_3TeO_6 using neutron diffraction measurements. A noncollinear spin arrangement of the Co spins is identified at low temperatures in the electrically polarized phase. The complex magnetic structure can be understood as resulting from the Co-O-Co superexchange (SE) interactions in significantly distorted CoO_6 octahedra and CoO_4 tetrahedra, where the Co ions crystallize into honeycomb and chain geometries.

III. PHENOMENOLOGICAL INTERPRETATION OF THE PHASES

In this section, we summarize our understanding of the various magnetic and ferroelectric phases observed in this system with a variety of experimental techniques and discuss the electromagnetic response in the various phases. A summary of the overall behavior is presented in Fig. 1. In the immediate vicinity of T_{M1}, one sees very small peaks in the (600) and (200) scattering as a function of temperature originating from critical scattering as the system initially orders, but no magnetic long-range order contribution to the CM peaks, which indicate the absence of long-range CM magnetic order, as indicated by both the previous neutron single-crystal measurements[5] and the present neutron powder data. The absence of magnetic order at the CM peaks indicates that the zero wave vector component of magnetic order is zero, or at least undetectable in the single crystal, that in contrast to interpretation of Ref. 1.

We assume it to be zero, in which case the phase transition at T_{M1} is undoubtedly continuous rather than weakly first order, as suggested in Ref. 7. This phase (A) supports only ICM long-range order at the star of $q = (q_h, q_k, q_l)$. Single-crystal data[5] combined with the present powder data fix the value of q to be weakly temperature dependent with a typical value in the region near (0.36, 0.12, 0.08). As discussed in the Appendix, (a) this phase is characterized by the complex-valued order parameters Q_A and Q_B associated with the two noncollinear wave vectors in the star of q and (b) one can have either a two-q state (which breaks the mirror symmetry) or a four-q state (which does not break mirror symmetry). In this phase, there is no long-range order in either the net magnetization or the spontaneous polarization. We remark that in phases like A, a two-q ordering is the most common type found experimentally. Thus, we assume that the four ICM diffraction peaks arise from having a multidomain sample. If so, by appropriately applying an external electric field, one can favor one domain over the other. When the electric field is removed, the energy favoring domain walls may be too small to reconstitute the multidomain structure. This technique (but involving a magnetic field) was used by Skanthakumar *et al.*[17] to identify the single-domain structure of Nd$_2$CuO$_4$. In the course of this domain enrichment process, one may observe changes in other properties such as the magnetic susceptibility, the dielectric susceptibility, and the strain tensor, which depend on the orientation of the axis of the ICM wave vector.

As the temperature is lowered through $T_{M2} = 19.5$ K, one enters phase B with the continuous emergence of the order parameter Q_4 at zero wave vector associated with the irrep Γ_4 so that the magnetic contributions to the Bragg intensities are

$$I_{020} = a\, Q_4^2, \quad I_{600} = b\, Q_4^2. \quad (1)$$

As discussed below, $b = 0$ implies that the moments are confined to the ac plane. As explained in the Appendix, the background ICM order can lead to a small admixture of the order parameter Q_2. Irrep Γ_4 (possibly with a small admixture of Γ_2) does not support either a net magnetic moment $\mathbf{M}(0)$ or a net spontaneous polarization $\mathbf{P}$. In phase B, an applied magnetic field $\mathbf{H}$ induces a nonzero $\mathbf{P}$ according to

$$P_b \propto Q_4 H_\perp, \quad P_\perp \propto Q_4 H_b, \quad (2)$$

where $\perp$ refers to components a or c. This conclusion follows from Table I and agrees with Ref. 7. Similarly, we predict that in phase B

$$M_b \propto Q_4 E_\perp, \quad M_\perp \propto Q_4 E_b. \quad (3)$$

A strong first-order phase transition into phase C occurs at $T_{M3} = 18$ K in agreement with Refs. 1, 3, and 5. As discussed in Sec. II, there are discontinuities in several independent parameters. Second-harmonic generation experiments of Ref. 7 indicate at $T = 5$ K (and presumably throughout phase C and D) the existence of domains having a magnetization perpendicular to the spontaneous polarization $\mathbf{P}$, which is collinear with the crystal b axis. The emergence of a nonzero P_b (at $\mathbf{H} = 0$) might be explained by the presence (additional to that of Q_4) of the order parameter Q_3 associated with irrep Γ_3.[18] To see that, note that $Q_3 Q_4$ is even under time reversal, and Table I indicates that this quantity transforms like P_b so

that $P_b = c Q_3 Q_4$, where c is a constant. Note that $Q_3 Q_4$ is related to the second-harmonic electric susceptibility χ_{ccc},[3] which shows a discontinuity at T_{M3}. Since Q_4 is already nonzero, this implies a discontinuity in Q_3. It would be nice to show that P_b turns on discontinuously at T_{M3} as our interpretation would imply. However, P_b is small enough that it is hard to observe directly.[3,7] In Ref. 1, phase C is said to support CM order at wave vector $(0, \frac{1}{2}, \frac{1}{4})$. As discussed above, our data contradict the presence of such order.

Now consider phase D. The only difference between this phase and phase C that has so far been experimentally clarified is that the ICM wave vector continuously develops a nonzero component q_k in phase D as T is lowered through T_{M4}. The properties of phase D, are, therefore, not very different from those of phase C. We do not attempt to give an interpretation of the unusual temperature dependence of the ICM wave vector, since that will probably require a complete understanding of the spin Hamiltonian.

Finally, we analyze the electric-field dependence of the order parameters in phase D. We assume the order parameters to be the Q_n at zero wave vector (see Table I). In terms of the Q_n, the magnetic contribution to the (020) intensity is

$$I_{020}(\mathbf{E}) = \alpha Q_3(\mathbf{E})^2 + \beta Q_4(\mathbf{E})^2, \quad (4)$$

where the coefficients are unspecified parameters (and similarly below). Experimentally, the second term is dominant. Thus, the linear (in $\mathbf{E}$) contribution to I_{020} is

$$\partial I_{020}/\partial E_\mu = 2\alpha Q_3(0)\partial Q_3/\partial E_\mu + 2\beta Q_4(0)\partial Q_4/\partial E_\mu. \quad (5)$$

In the absence of magnetic ordering the scattering intensities are even functions of the electric field $\mathbf{E}$. The $\mathbf{E}$ dependence of the Q_n is determined by the free energy

$$F = \frac{1}{2}\sum_n \chi_n^{-1}[Q_n(\mathbf{E}) - Q_n(0)]^2 + \delta F, \quad (6)$$

where χ_n is the susceptibility associated with Q_n and δF contains coupling terms involving $\mathbf{E}$ and Q_n. Coupling terms such as $E_\mu Q_n$ are not time-reversal invariant and hence are not allowed. Using Table I, we find that to lowest order in $\mathbf{E}$

TABLE I. Symmetry of the order parameters Q_n for the magnetic (odd under time reversal) irreps Γ_n at zero wave vector for Co$_3$TeO$_6$ and of the electric field $\mathbf{E}$ (or equivalently the polarization) vector. The symmetry labels of the irreps are $C2/c$ for Γ_1, $C2/c'$ for Γ_2, $C2'/c'$ for Γ_3, and $C2'/c$ for Γ_4. Our numbering of the irreps agrees with that of the website ISODISTORT and with Ref. 5, but not with Ref. 7. In any event, our labeling of the irreps is defined by their eigenvalues. Here, $\lambda(O)$ is the eigenvalue of the operator O: $O Q_k = \lambda(O) Q_k$. Also, E is the identity, and I is spatial inversion. In the last line, we give the direction of the ferromagnetic moment, if it is allowed to be nonzero.

	Q_1	Q_2	Q_3	Q_4	$E_\perp$	E_b
$\lambda(E)$	+1	+1	+1	+1	+1	+1
$\lambda(2_b)$	+1	+1	−1	−1	−1	+1
$\lambda(m_b)$	+1	−1	−1	+1	+1	−1
$\lambda(I)$	+1	−1	+1	−1	−1	−1
M	**B**	0	$\perp \mathbf{b}$	0	—	—

and Q, δF must be of the form

$$\delta F = a' E_\perp Q_1 Q_4 + b' E_\perp Q_2 Q_3 + c' E_\parallel Q_1 Q_2 + d' E_\parallel Q_3 Q_4 \tag{7}$$

in terms of the components of the electric field perpendicular and parallel to the b axis. Mininizing F with respect to Q_4 leads to

$$0 = \chi_4^{-1}[Q_4(\mathbf{E}) - Q_4(0)] + a' E_\perp Q_1 + d' E_\parallel Q_3, \tag{8}$$

so that

$$\partial Q_4 / \partial E_\parallel = -\chi_4 d' Q_3(0), \quad \partial Q_4 / \partial E_\perp = -\chi_4 a' Q_1(0). \tag{9}$$

Minimizing F with respect to Q_3 leads to

$$0 = \chi_3^{-1}[Q_3(\mathbf{E}) - Q_3(0)] + b' E_\perp Q_2 + d' E_\parallel Q_4, \tag{10}$$

so that

$$\partial Q_3 / \partial E_\parallel = -\chi_3 d' Q_4(0), \quad \partial Q_3 / \partial E_\perp = -\chi_3 b' Q_2(0). \tag{11}$$

Thus,

$$\begin{aligned} I_{020}(E) = {}& I_{020}(0) - 2\beta a' \chi_4 Q_4(0) Q_1(0) E_\perp \\ & - 2\alpha b' \chi_3 Q_3(0) Q_2(0) E_\perp \\ & - 2[\alpha d' \chi_3 + \beta d' \chi_4] Q_3(0) Q_4(0) E_\parallel. \end{aligned} \tag{12}$$

Since $|Q_2(0)| \ll |Q_4(0)|$ and $|Q_1(0)| \ll |Q_3(0)|$, the largest effect occurs when the field is parallel to the b axis. However, the effect is not very large because the spontaneous polarization is small, and as we will see from the fit of Fig. 5, we know that $Q_3(0)$ must not be large. Although a convincing general analysis is difficult, we believe that the fact that at $\boldsymbol{E} = 0$ one has $I_{600} = 0$ implies that for small $\boldsymbol{E}$ one has $I_{600} \propto \boldsymbol{E}^2$.

As mentioned above, the two scenarios which would explain a spontaneous polarization involve having (a) two different zero wave vector irreps or (b) two copies of the single irrep of the nonspecial IC wave vector. Only in the latter case would the ICM magnetic reflections have a linear dependence on the electric field, because, as mentioned above, there are no terms linear in the order parameter and the electric field. Thus, the fact that the ICM reflections show no dependence on the electric field is evidence that we only have a single copy of the ICM order parameter and therefore that the spontaneous polarization is not caused by the ICM magnetic order.

IV. SAMPLE FABRICATION

Single crystals of Co_3TeO_6 were synthesized via chemical vapor transport redox reactions.[2] The Co_3O_4, TeO_2, and $CoCl_2$ powders were mixed thoroughly using a molar ratio of 4:3:1 before being loaded into one end of a silica tube. The tube was then evacuated to 10^{-5} torr, and filled with HCl gas that acts as the transporting agent, before being sealed off. The ampoule was subsequently placed in a two-zone furnace, with the temperatures of the charge and growth zones set to 973 and 873 K, respectively. This allowed the transportation of the starting materials from the charge zone to epitaxially grow into single crystals in the growth zone. The resultant single crystals were dark violet in color. The single crystal used in the present measurements weighed 101 mg, with a size of $14.1 \times 2.2 \times 0.9$ mm^3. A number of small crystals were crushed into powder for x-ray and neutron powder diffraction measurements. X-ray diffraction was first used to check the powdered sample. No obvious differences were found in the x-ray diffraction patterns taken from different portions of the powdered sample.

V. NEGATIVE THERMAL EXPANSION

Neutron and x-ray powder diffractions were used to determine the crystalline structure. The high-resolution neutron powder diffraction patterns were collected on BT-1, a 32-detector powder diffractometer at the National Institute of Standards and Technology Center for Neutron Research, using Ge(311) monochromator crystals to define an incident wavelength of 2.078 Å. Angular collimators with horizontal divergences of 15′, 20′, and 7′ full width at half-maximum (FWHM) acceptance were used for the in-pile, monochromatic, and diffracted beams, respectively. For these measurements, $\sim$6 g of the sample were loaded into a cylindrical vanadium can that gave rise to no measureable neutron diffraction peaks. The high-resolution synchrotron x-ray powder diffraction patterns were collected on the BL01C2 beam line at the Taiwan National Synchrotron Radiation Research Center, using an incident wavelength of 0.77495 Å, as defined by a Si(111) double-crystal monochromator. The diffraction intensities were recorded by a Mar345 imaging plate system, with a sample-to-detector distance of 300 mm. The sample temperature was controlled using a He-gas closed-cycle refrigerator system, equipped with a high power heater. Uncertainties where indicated throughout are statistical in origin and represent one standard deviation.

The diffraction patterns were analyzed using the General Structure Analysis System program,[19] following the Rietveld profile refining method. The high-resolution neutron diffraction pattern taken at 30 K can be described assuming the same monoclinic $C2/c$ (No. 15, b unique) symmetry reported[2,3] for the compound at room temperature. The complex crystalline structure of Co_3TeO_6 can be viewed as being composed of six distorted Co_3Te layers (the crystallographic b-c plane) that are interconnected through O ions along the longest crystallographic a axis direction. The bond valence calculation indicates that all Co ions are divalent. The interlayer bonding occurs through O ions that form corner-, edge-, and face-sharing CoO_6 octahedra and CoO_4 tetrahedra, which provide an antiferromagnetic Co-O-Co SE path for the Co spins. The TeO_6 octahedra, on the other hand, are isolated from each other but fill the spatial gaps between the CoO_6 octahedra.

Although optical second-harmonic generation measurements[3] suggest a breaking of structural symmetry occurs at 18 K, this structural distortion or change cannot be identified in our high-resolution neutron and synchrotron x-ray diffraction measurements, which reveal a negative thermal expansion during the ferroelectric transition. Figure 2 illustrates the variations of lattice parameters with temperature below 35 K. No magnetic correlations are detected at 35 K and above. All three lattice constants and the incline angle of the monoclinic unit cell display the same thermal profile, revealing a dip at 18 K. They shrink a very significant 0.02% upon cooling from
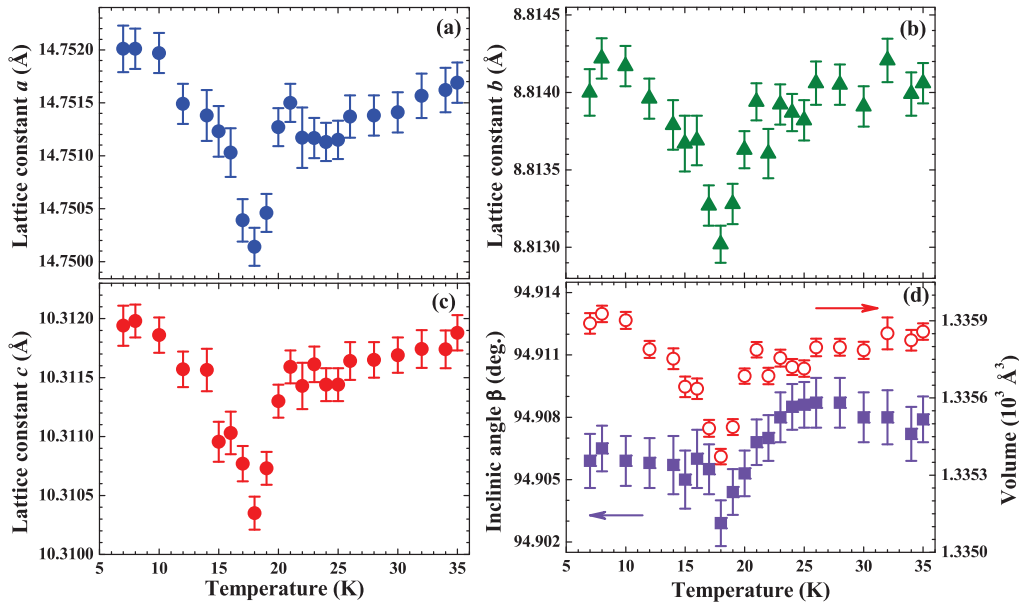
FIG. 2. (Color online) Temperature dependencies of the (a) lattice constant a, (b) lattice constant b, (c) lattice constant c, and (d) incline angle and unit cell volume of the crystalline unit cell of Co_3TeO_6. All three lattice parameters, the incline angle, and unit cell volume display the same thermal variation profile in this temperature regime. Negative thermal expansion of the crystalline unit cell appears between 10 and 18 K.

20 to 18 K, when the CM magnetic ordering develops.[3–5] Similar variations in the lattice parameters have also been reported in a separate study.[1] It is not common to have the lattice coupled this strongly to spin ordering. Magnetic couplings in Co_3TeO_6 are mainly from the wave function overlap between the Co and O ions in the Co-O-Co SE paths. Lattice shrinkage resulting from wave function overlap is understandable, but a 0.02% lattice reduction within a temperature change of 2 K is surprising. On the other hand, the lattice expands upon cooling during the development of electrical polarization between 18 and 16 K. It is interesting to note that the alignment of electrical polarization pushes the neighboring ions significantly further apart along all three crystallographic directions rather than along a particular axis direction. All these behaviors reveal that both the electric and magnetic order parameters are strongly coupled to the lattice. We remark that although lattice anomalies associated with multiferroic transitions have been observed in other type-II multiferroics, such as $TbMn_2O_5$,[12] $HoMn_2O_5$,[12] $Ni_3V_2O_8$,[20] and $GdMnO_3$,[21] sizeable negative thermal expansion along all three crystallographic axis directions that is directly linked to the ferroelectric transition is rarely found.

VI. LOW-TEMPERATURE SPIN ARRANGEMENT

The five crystallographically distinct Co ions crystallize into two different layered arrangements. One is linked with Te ions, and the other contains only Co. Figure 3 illustrates the network of severely distorted Co-Te layers, which is viewed along the $[\bar{1}01]$ direction, but for clarity without the presence of the interconnecting O ions. Four separate layers (marked A, B, C, D) may be distinguished in a unit block, and the whole structure may be obtained by translating the unit block along the a axis direction. Layers C and D can

be reached by a translation operation of layers A and B, respectively, through $(a/2\ b/2\ 0)$. The Co ions in layer A construct a significantly distorted honeycomb, with Te(1) or Te(2) occupying the centers. Together with the interconnecting O ions, located between but somewhat above them, these Co-Te-O ions form wavy, distorted honeycomb webs that propagate the magnetic correlations. Layer B is composed
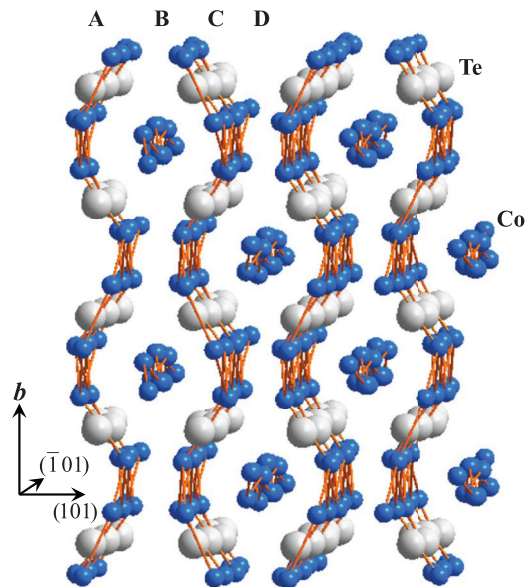
FIG. 3. (Color online) Networking of the severely distorted Co/Te layers viewed along the $(-1\ 0\ 1)$ axis direction, without the presence of interconnecting O ions for clarity. The layers marked C and D can be reached by a translation operation of the layers marked A and B, respectively, through $(a/2\ b/2\ 0)$. The Co(1)-Co(4) chains lie along the $[1,0,-1]$ direction.
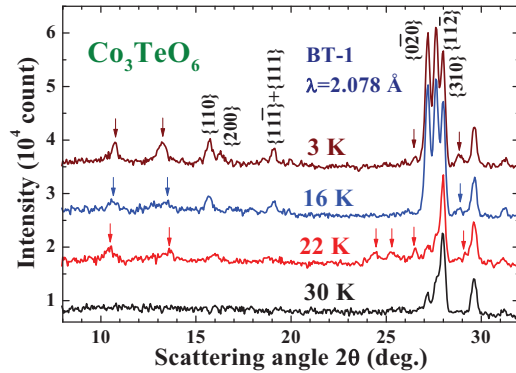
FIG. 4. (Color online) Direct comparison of the low-angle portions of the high-resolution neutron powder-diffraction patterns collected at four representative temperatures. The diffraction intensities observed at 30 K are from the crystalline structure. Additional intensities at the ICM positions, indicated by arrows, appear in the patterns taken at 22 K and below. Magnetic intensities at the CM positions are revealed in the patterns taken at 16 and 3 K.

FIG. 5. (Color online) Observed (crosses) and fitted (solid lines) high-resolution neutron powder-diffraction patterns taken at 3 K, assuming a monoclinic $C2/c$ symmetry for the crystalline structure, a $C2'/c$ magnetic symmetry for the Co spins, plus an ICM magnetic component. The differences between the calculated and observed patterns are plotted at the bottom. The three sets of solid vertical lines mark the calculated positions of the Bragg reflections of the proposed crystalline, magnetic, and ICM structure.

of well-separated Co(1)-Co(4)-Co(4) zigzag chains. Each neighboring pair of Co ions is interconnected through O ions as well. There is no direct bonding between neighboring chains. The Co-O bond lengths and Co-O-Co bond angles in both layers A and B vary widely. Their differences can be as large as 50%, which results in widely varying magnetic interactions that compete within the unit cell.

The development and evolution of magnetic order can be seen in Fig. 4, where low-angle portions of the neutron powder diffraction patterns taken at four representative temperatures are displayed together for direct comparison. All the Bragg reflections observed at 30 K can be associated with the monoclinic $C2/c$ crystalline structure. Weak but definitive magnetic reflections are seen at the ICM positions (arrows in Fig. 4) at 22 K, in good agreement with our previous detailed single-crystal measurements.[5] No detectable change in the intensities at the CM positions can be identified at this temperature, in agreement with the previous single-crystal data, indicating there is no change in the crystal structure and no CM component of the magnetic structure in this temperature range. On further cooling to 16 K, additional intensities at the CM positions are clearly revealed, where the ICM intensities shift to a new wave vector as well. The ICM intensities undergo another transition again into the ground state with a different wave vector. The behavior of the ICM wave vector ordering is in a good agreement with the single-crystal diffraction study as a function of both temperature and magnetic field.[5]

Adopting the $C2/c$ crystalline symmetry of the Co ions, there are then eight possible magnetic space groups for the 36 Co spins in the magnetic unit cell. The goodness of fit to the neutron pattern taken at 3 K is apparently much better when assuming a $C2'/c$ (Γ_4) symmetry for the Co spins, where the prime indicates the time-reversal operation. In addition to the CM reflections, there are several peaks at low angles that require an ICM wave vector for their description. It is clear that it is not possible to uniquely determine the modulation wave vector $\vec{q}$ of these ICM reflections based solely on the powder data, but our previous single-crystal measurements[5] made in the $(h, k, 0)$ scattering plane (obtained from the same batch as

for the present single-crystal-crushed powder sample) identified $q_h = 0.357$ and $q_k = 0.103$ at 3 K. With this additional information, the powder pattern taken at 3 K was then refined using the FullProf program,[22] which allows ICM analysis.

Figure 5 shows the observed (crosses) and calculated (solid lines) patterns at 3 K, assuming the $C2/c$ symmetry for the monoclinic crystalline structure, the $C2'/c$ symmetry for the Co spins, plus an ICM component of modulation vector $\vec{q}$. They agree very well. An l component for $\vec{q}$ is needed for a better description of the powder pattern at 3 K. The modulation vector thus obtained is $\vec{q} = (0.357, 0.103, 0.087)$. The crystalline parameters thus obtained for the present Co_3TeO_6 at 30 K are summarized in Table II. Figures 6(a) and 6(b) illustrate the proposed spin arrangements in layer A and layer B, respectively. The spin arrangement of layer C and layer D can be obtained by translation operations from layers A and B, respectively, through $(a/2 \ b/2 \ 0)$. The magnetic moments and their components along the three crystallographic axis directions of the five distinct Co ions are tabulated in Table III. There is no constraint introduced to the magnetic moment of an individual Co ion during the initial refinements. It appears that the moments of the Co ions in layer A [Co(2), Co(3), and Co(5)] have the same magnitude of $\langle \mu_Z \rangle = 2.68(3) \mu_B$, or they differ too little for detection at our sensitivity. The moments lie in the ac plane but point either $40°$ away from the a axis direction or along the opposite direction to form a simple antiferromagnetic arrangement. Likewise, each of the Co ions in layer B, that is, the Co(1)-O-Co(4)-O-Co(4) zigzag chains, carries a moment of $\langle \mu_Z \rangle = 2.10(4) \mu_B$. They also lie in the ac plane, but form a noncollinear spin arrangement, with the moments pointing nearly along the [101] direction or its conjugate directions.

It is very interesting to find that only the Co ions in layer B [Co(1) and Co(4)] contribute to the ICM intensities, whereas those in layer A carry no ICM moment. Refinements that force the Co ions in layer A to carry detectable ICM moments result in much poorer fits (dashed curves), as shown in Fig. 7.

TABLE II. Refined lattice parameters and atomic positions of Co$_3$TeO$_6$ at 30 K, assuming a symmetry of space group $C2/c$ ($Z = 12$).

Co$_3$TeO$_6$, $T = 30$ K, $\chi^2 = 0.9983$; $R_{wp} = 3.41\%$; $R_p = 2.77\%$				
$a = 14.7789(3)$ Å, $b = 8.8293(1)$ Å, $c = 10.3321(2)$ Å, $\alpha = 90°$, $\beta = 94.943(2)°$, $\gamma = 90°$				
Atom	Site	X	Y	Z
Te(1)	$4b$	0	0.5	0.5
Te(2)	$8f$	0.6610(4)	−0.5030(11)	0.2974(4)
Co(1)	$4e$	0.5	−0.1785(24)	0.25
Co(2)	$8f$	0.8582(7)	−0.3571(17)	0.2363(12)
Co(3)	$8f$	0.5227(8)	−0.6543(17)	0.0416(10)
Co(4)	$8f$	0.6582(10)	−0.2969(13)	0.0595(13)
Co(5)	$8f$	0.8002(9)	−0.3633(14)	0.5720(12)
O(1)	$8f$	0.92751(42)	−0.3357(8)	0.5611(7)
O(2)	$8f$	0.59421(40)	−0.3468(8)	0.2037(6)
O(3)	$8f$	0.60191(42)	−0.6557(9)	0.1987(7)
O(4)	$8f$	0.74822(33)	−0.5267(7)	0.6678(5)
O(5)	$8f$	0.92935(36)	−0.5134(10)	0.3361(4)
O(6)	$8f$	0.58197(34)	−0.5100(10)	0.4373(5)
O(7)	$8f$	0.92689(47)	−0.6590(7)	0.5655(7)
O(8)	$8f$	0.73833(43)	−0.3463(11)	0.3935(7)
O(9)	$8f$	0.72739(40)	−0.6631(8)	0.3883(6)

The differences can be revealed by examining the intensity ratio between the $\{001\}^-$ and $\{110\}^- + \{001\}^+ + \{200\}^-$ reflections. The fitted intensity ratios for the two reflections when assuming the Co spins in layer A that do not and do carry ICM moments are 0.92 (solid curves) and 0.43 (dashed curves), respectively, whereas the observed one is 0.83. The proposed model with only Co(1) and Co(4) carrying ICM moments agrees with the fact that the Co spins in layer A form a simple antiferromagnetic arrangement that contributes insignificantly to the ICM order. This is also consistent with the observation that the ICM and CM orders develop at different temperatures. The ICM order is thus mainly linked to the noncollinear spins in the Co(1)-O-Co(4)-O-Co(4) frustrated zigzag chains. A $\vec{q} = (0, 0.5, 0.25)$ for the ICM wave vector, with all Co ions contributing to the ICM component, has been suggested in a separate study[1] based on neutron powder diffraction data. Our powder data (Fig. 5) fit equally well with that model. There are indeed many sets of $(q_h\ q_k\ q_l)$ which fit reasonably well to the three ICM peaks observed in the powder data alone, but in the present analysis q_h and q_k are known from the single-crystal measurements so that q_l is the only fitting parameter. Determination of just q_l using the powder data is then feasible.

The distinct spin arrangements obtained for the Co spins in layers A and B are naturally connected to their distinct crystallographic geometry. The Co ions in layer A form a severely distorted honeycomb web, with the Te ions located in the channels. There are three adjacent Co neighbors for each Co ion. Each pair of neighboring Co ions is interconnected through the O ions located between but above or below them. The geometries of the Co-O-Co SE paths associated with crystallographically distinct Co ions [Co(2), Co(3), and Co(5)] are different but all with a relatively long Co-Co separation (3.45 Å on average) and a relatively large Co-O-Co bond angle (117 or 94°). The magnetic coupling is
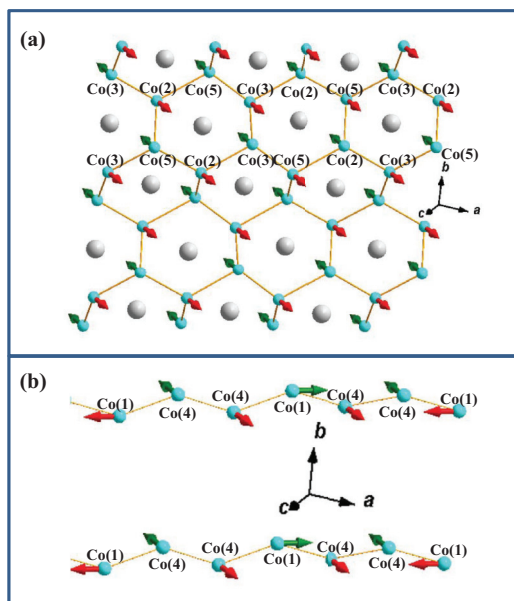
FIG. 6. (Color online) Schematic drawing of the proposed Co spin arrangements in (a) layer A and (b) layer B. The Co spins in the wavy honeycomb web form a simple antiferromagnetic arrangement; whereas those in the zigzag chains form a noncollinear spin arrangement. The moments of all Co ions lie in the ac plane.

TABLE III. Magnetic moments of the five crystallographically distinct Co ions, obtained assuming a magnetic space group of $C2'/c$, where CN represents the coordinate number that indicates the number of surrounding O ions.

Ion	CN	m_a (μ_B)	m_b (μ_B)	m_c (μ_B)	$\langle \mu_Z \rangle$ (μ_B)
Co(1)	6	−1.43(5)	0	1.55(4)	2.10(4)
Co(2)	6	1.73(5)	0	2.04(3)	2.68(3)
Co(3)	6	−1.73(5)	0	−2.04(3)	2.68(3)
Co(4)	6	1.43(5)	0	1.55(4)	2.10(4)
Co(5)	4	1.67(9)	0	2.04(3)	2.64(5)
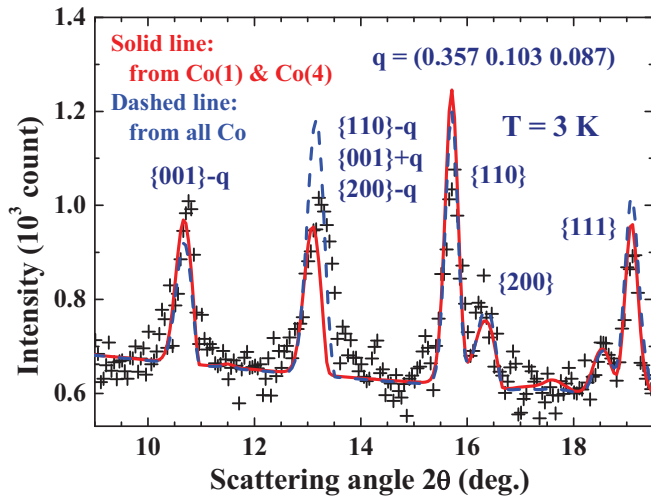
FIG. 7. (Color online) Direct comparison of the results of fits assuming the Co spins in the honeycomb web do contribute (dashed curves) and do not contribute (solid curves) to the ICM moments. The calculated intensity for the ICM reflections at $13.2°$ is substantially stronger than the observed one when ICM moments on the Co ions in layer A are imposed.

thus mainly through antiferromagnetic SE paths. Theoretical studies[23,24] based on the quantum J_1-J_2-J_3 model, which includes interactions from the first J_1, second J_2, and third J_3 neighboring pairs in honeycomb lattices, have found a simple antiferromagnetic ground state for the cases of small frustration whenever J_2/J_1 or J_3/J_1 is less than 0.15. The simple antiferromagnetic spin arrangement together with no ICM component found in layer A indicates that there is no significant magnetic frustration appearing in these layers. Perhaps the Te ions at the centers of the honeycomb do indeed interrupt or block the secondary magnetic interactions among the Co spins. Collinear spin arrangements in a Co-O-Co geometry with a relatively long Co-Co separation have also been observed in CoO (3.530 Å),[25] Co_3O_4 (3.5461 Å),[26] and Co_2SiO_4 (3.8757 Å).[27] On the other hand, the noncollinear spin arrangement together with the appearance of an ICM component for the Co(1)-O-Co(4)-O-Co(4) zigzag chains in layer B show that they experience a more complicated magnetic coupling. This could be because the Co-Co separations in the zigzag chains are significantly shorter (3.30 Å on average) so that the secondary interactions are also evidently revealed in addition to the indirect Co-O-Co SE interactions. We remark that the proposed magnetic structure can generate two separate spin-flop transitions,[4,5] one from the Co spins in layer A and the other from those in layer B.

One important point to note is that the proposed Γ_4 symmetry for the CM magnetic order generates no magnetic intensity for the (600) reflection, which disagrees with our previous interpretation of the single-crystal data, where a strong temperature dependence was observed at both T_{M3} and T_{M4} (see Fig. 3 of Ref. 5). However, the present powder results show no significant temperature dependence of the (600) intensity [as we will see in Fig. 10(b)], nor is there any significant temperature dependence obtained for the present data on the single crystal when aligned for the [$h0l$] scattering plane [Fig. 10(b)]. In addition, although the powder data do
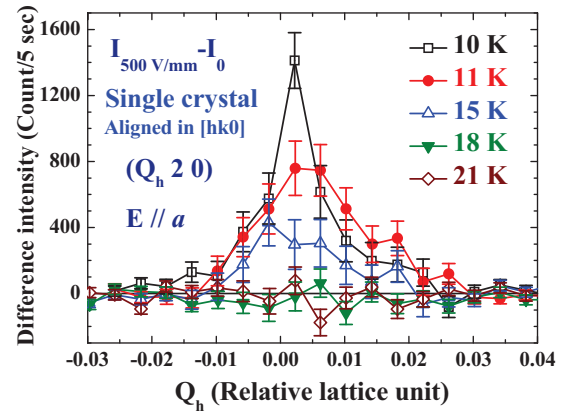
FIG. 8. (Color online) Difference intensities for the (020) reflection taken with and without an electric field of strength 500 V/mm applied along the *a* axis direction, measured at five representative temperatures. The difference intensities begin to develop below 18 K. The measurements were performed with the crystal aligned for the [$hk0$] scattering plane.

not have the sensitivity to distinguish T_{M2} from T_{M3}, there is no clear evidence for T_{M4} in the temperature dependence curve of the (020) reflection obtained on the powder sample as will be shown in Fig. 9(b). The question is then, what are the sources of the anomaly T_{M3} revealed in Fig. 8 and Ref. 5. We believe that this intensity change originates for the relief of (likely primary) extinction in the crystal,[28–31] as the powder data demonstrate that it is not of magnetic origin, nor are there structural changes large enough to detect directly in either the x-ray or neutron powder diffraction measurements. We note that extinction for a single crystal depends on the perfection, shape, and thickness of the crystal, and, of course, on the strength of the Bragg peak. The (600) is a strong peak, with a calculated intensity that is ∼19 times higher than the (020) peak, for example, and the extinction being relieved attests to the high perfection of this single crystal. On the other hand, it is clear that the intensity change is associated with a transition in the crystal, but with a distortion too small to detect in via high-resolution powder diffraction. We note that on cooling the electric polarization begins to develop at T_{M3} and becomes saturated at T_{M4},[4,5] and it may be the formation of ferroelectric domains in the crystal that triggers the relief of extinction.

VII. EFFECTS OF AN APPLIED ELECTRIC FIELD

The effects of an applied electric field on the magnetic intensity were studied using the single-crystal sample. These measurements were conducted on the thermal triple-axis spectrometer TAIPAN at Australian Nuclear Science and Technology Organization, using pyrolytic graphite PG(002) monochromator crystals and analyzer crystals to define a wavelength of 2.35 Å for the incident as well as the scattered neutrons. Angular collimators with horizontal divergences of 80′, 40′, 40′, and 120′ FWHM acceptance were used for the in-pile, monochromatic, diffracted, and analyzed beams, respectively. The electric field, applied along the *a* axis direction, was furnished by two aluminum electrodes, separated by 1.5 mm and electrically isolated by a piece of Macor, with a
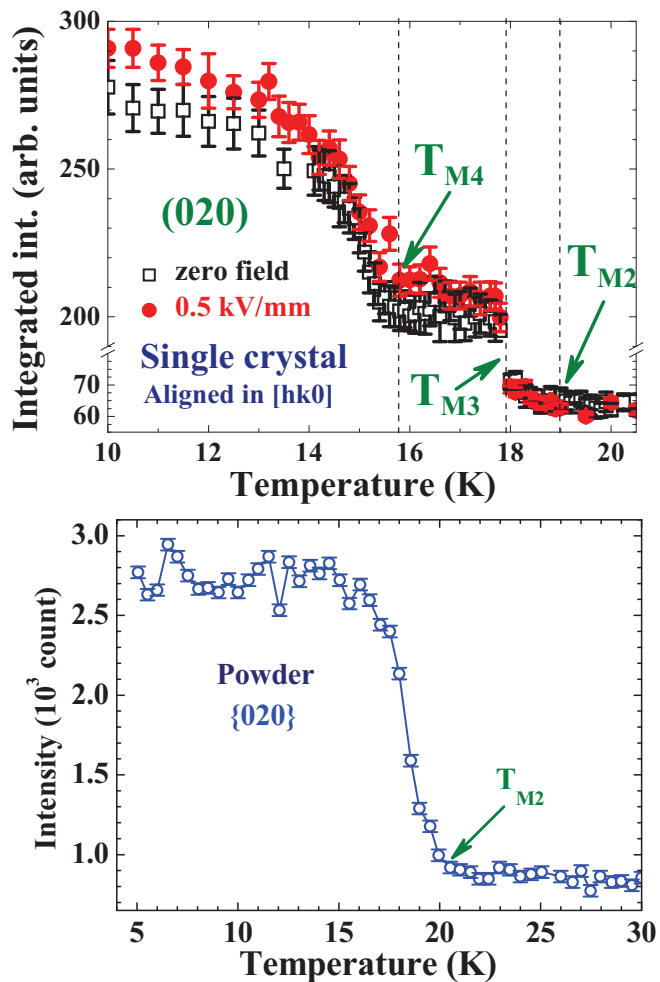
FIG. 9. (Color online) (a) Temperature dependence of the single crystal (020) integrated intensity aligned in the [$hk0$] scattering plane, taken with (filled circles) and without (open squares) an electric field of strength 500 V/mm applied along the a axis. The (020) intensity is noticeably enhanced by the applied electric field below T_{M3}. (b) Temperature dependence of the {020} reflection taken on the powder sample. T_{M2} is clearly revealed but T_{M3} and T_{M4} are not. This intensity increase is magnetic in origin. The jump in scattering at 18 K in the top panel is likely structural and may originate from the relief of extinction at this transition.

dielectric strength of 62.4 kV/mm. The sample temperature was controlled using a He-gas closed-cycle refrigerator system.

It has been reported[3] that the electric polarization of Co$_3$TeO$_6$ can be noticeably enhanced by an applied magnetic field. It is interesting to find that the magnetic order parameter can also be altered by an electric field $\boldsymbol{E_a}$. Figure 8 displays the difference intensities between the (020) reflection measured at $E_a = 0$ and 500 V/mm along the a axis direction, taken at five representative temperatures. At 21 and 18 K, an $E_a =$ 500 V/mm along the a axis direction produces no detectable effect on the (020) reflection. At 15 K, increases of the (020) intensity are clearly seen, and the increases are enhanced at lower temperatures.

Figures 9(a) and 10(a) illustrate the effects of $E_a = 500$ V/ mm, applied along the a axis direction, on the temperature
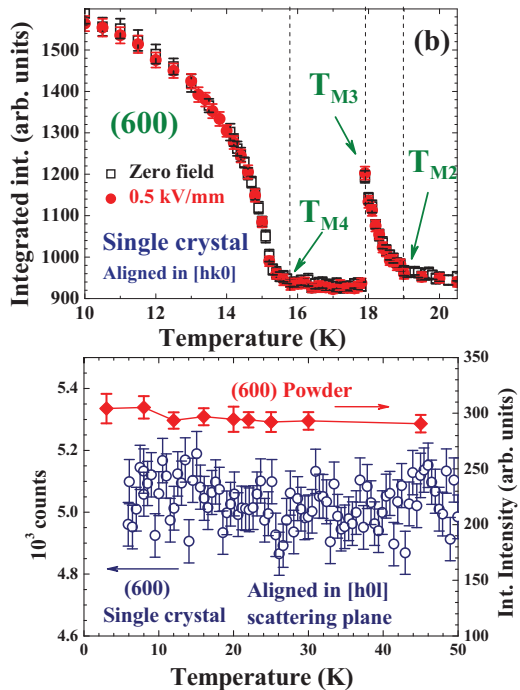
FIG. 10. (Color online) (a) Temperature dependence of the single-crystal (600) integrated intensity aligned in the [$hk0$] scattering plane, taken with (filled circles) and without (open squares) an electric field of strength 500 V/mm applied along the a axis. Note that the temperature dependence here is structural in origin and likely originates from the relief of extinction. No detectable change is found in the (600) intensity with electric field. (b) Temperature dependence of the {600} reflection taken on the powder sample (filled squares) and on the single crystal (open circles) aligned in the [h0l] scattering plane. No significant variation of the intensity is detected in the temperature range studied.

dependencies of the (020) and (600) intensities, respectively. These single-crystal Bragg intensities were measured with the crystal aligned in the [$hk0$] scattering plane. The temperature profile of the two peaks and the three transition temperatures (marked T_{M2}, T_{M3}, and T_{M4}) are essentially unaffected by this applied electric field. In addition, T_{M1} is also unaffected by the E_a (data not shown). Nevertheless, the (020) intensities are noticeably enhanced at temperatures below T_{M3} but not above, as can be seen in Fig. 9(a). No additional enhancement in the (020) intensity is detected when a higher E_a of 2 kV/mm is applied. Note that T_{M3} is the temperature below which spontaneous electrical polarization develops.[3–5] On the other hand, the (600) intensities are essentially unaffected by the application of E_a, as shown in Fig. 10(a) and remain insensitive up to the highest E_a achieved in this study of 2 kV/mm. As mentioned below Eq. (12) we believe that $I(600) \propto \boldsymbol{E}^2$ explains why the dependence of $I(600)$ on the electric field is too small to detect experimentally. It is known that the magnetic intensity of a reflection (hkl) is associated with the components of the moments that are perpendicular to the reciprocal vector. The observations that the (020) but not the (600) intensities are enhanced by E_a along the a axis direction indicate that the moments along the a axis direction can indeed be enhanced by E_a once the electric polarization
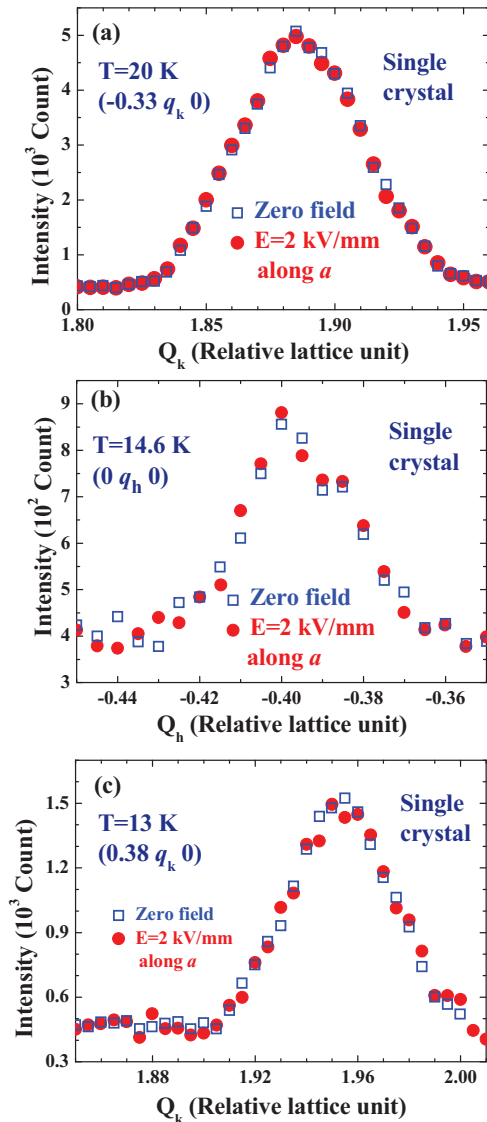
FIG. 11. (Color online) Direct comparison of the three ICM reflections (a) $(-0.33\ 1.87\ 0)$, (b) $(0\ -0.40\ 0)$, and (c) $(0.38\ 1.95\ 0)$, taken with (filled circles) and without (open squares) an electric field of strength 2 kV/mm applied along the *a* axis direction. No detectable change in the diffraction intensity is seen in all three ICM reflections.

develops. This enhancement demonstrates directly that Co_3TeO_6 is a type-II multiferroic, where the magnetic and electric degrees of freedom are coupled. The ICM intensities are not affected by the application of an E_a up to 2 kV/mm along the *a* axis direction. Figure 11 displays three representative ICM reflections, taken without (open squares) and with $E_a = 2$ kV/mm (filled circles). There is no detectable difference in the intensity and peak position between the peaks measured with and without $\boldsymbol{E}$.

VIII. DISCUSSION AND CONCLUSIONS

The Co ions in layer A crystalize into a severely distorted honeycomb structure. The collinear antiferromagnetic arrangement found for these Co spins shows that magnetic frustration, if it does exist from the higher-order interactions, is insignificant in driving the spin arrangement. Based on the quantum J_1-J_2-J_3 model calculation,[24] a simple collinear spin arrangement can be expected when the strength of magnetic frustration is within 15% of the main magnetic interactions. It appears that the accommodation of nonmagnetic Te ions at the centers of the honeycomb blocks or reduces the higher-order magnetic interactions, which stabilizes the spin arrangement driven by the antiferromagnetic Co-O-Co SE interactions. On the other hand, the Co ions in layer B form well-separated zigzag chains, with no Te ions nearby. A noncollinear spin arrangement is found for the Co ions in layer B, and they contribute an additional ICM moment as well. The two distinct spin structures found in layers A and B agree with the fact that two spin-flop transitions initiated by applied magnetic field can occur.[4]

The magnetoelectric effect (in which a spontaneous polarization $\boldsymbol{P}$ is induced by magnetic order) in type-II multiferroic systems with a spiral spin structure can now be understood[32,33] on the basis of the spin-current model,[34] which argues that the spin current induced by two nonparallel spins gives rise to a nonzero electric dipole moment. These local dipole moments lead to a nonzero $\boldsymbol{P}$ assuming a permissible crystal symmetry. This implies that the magnetic order can be modified by an applied electric field. Both the CM and ICM magnetic components of $Ni_3V_2O_8$,[35] $LiCu_2O_2$,[36] and $TbMnO_3$ (Ref. 37) have been found to be sensitive to an external electric field. In Co_3TeO_6, the ICM component is insensitive to an electric field up a strength of 2 kV/mm applied along the *a* axis direction. The enhancement in the CM component by the applied electric field is small ($\sim$5%) and reaches saturation at 500 V/mm and only the *a* axis moment is affected.

In the Landau picture, a nonzero $\boldsymbol{P}$ is usually attributed to a trilinear interaction involving the coupling of two different irreps to $\boldsymbol{P}$. If the zigzag chains are responsible for the nonzero $\boldsymbol{P}$, one would instead invoke two copies of the same (one dimensional) irrep at the ICM wave vector.[18] However, the fact that the ICM magnetic order is insensitive to the electric field means that either the nonzero $\boldsymbol{P}$ is not to be attributed to the zigzag chains, or that their magnetic order is dependent on the electric field, but with a dependence that is too weak for our experiments to observe. An alternative interpretation is to attribute the nonzero $\boldsymbol{P}$ to the honeycomb web of the Co(2)-Co(3)-Co(5) spins. In this interpretation, the weak $\boldsymbol{P}$ would, in the spin-current model, be attributed to a small noncollinearity of the web spins due to the introduction of small component of the Γ_3 irrep. Since the trilinear coupling of Landau theory is proportional to $Q_3Q_4|\boldsymbol{P}|$, it would lead to the same conclusion. The advantage of this interpretation is that it would explain the weak dependence of the (020) intensity on the electric field. The disadvantage of this interpretation is that the instrumental resolution and statistical accuracy are not sufficient to distinguish a Γ_4 structure from a $\Gamma_3 \times \Gamma_4$ structure. In the future, a detailed polarization analysis study might reveal additional details of the magnetic and nuclear structure to unambiguously settle this question.

Note added in proof. Recently, we found Ref. 38 by H. Singh *et al.*, which provides evidence in support of this magnetoelectric ordering.

APPENDIX: EFFECT OF ICM ORDERING ON CM IRREPS

The symmetry operations (apart from translations) of the paramagnetic crystal are

$$E = (x,y,z), \quad I = (\bar{x},\bar{y},\bar{z})$$
$$2_b = \left(\bar{x},y,\bar{z}+\tfrac{1}{2}\right) \quad m_b = \left(x,\bar{y},z-\tfrac{1}{2}\right). \quad \text{(A1)}$$

In terms of ICM amplitudes Ψ at the star of the nonspecial wave vector (h,k,l), the spin function can be written as

$$\Psi = Q_A\,\Psi(h,k,l) + Q_A^*\,\Psi(\bar{h},\bar{k},\bar{l}) + Q_B\,\Psi(h,\bar{k},l)$$
$$+ Q_B^*\,\Psi(\bar{h},k,\bar{l}). \quad \text{(A2)}$$

The complex-valued amplitudes Q_A for wave vector (h,k,l) and Q_B for wave vector, $(h,\bar{k},l)$ are the order parameters that describe ICM magnetic order. Since applying a symmetry operation to a spin function does not change its normalization, these operations only introduce phase factors. We may define the phase of the order parameters such that

$$I\,Q_x = Q_x^*, \quad 2_b\,Q_x = \xi\,Q_{\bar{x}}^*, \quad m_b\,Q_x = \xi\,Q_{\bar{x}}, \quad \text{(A3)}$$

where $\xi \equiv \exp(\pi i l)$, $\bar{A} = B$ and $\bar{B} = A$. From translational invariance (wave vector conservation), we see that the free energy can only involve the combinations $|Q_A|^2$ and $|Q_B|^2$, for which

$$I|Q_X|^2 = |Q_X|^2, \quad 2_b|Q_X|^2 = |Q_{\bar{X}}|^2, \quad m_b|Q_X|^2 = |Q_{\bar{X}}|^2. \quad \text{(A4)}$$

Initially, we ignore the coupling between CM and ICM orders, and up to quartic order the free energy F is

$$F = \frac{1}{2}[T - T_q][|Q_A|^2 + |Q_B|^2] + u[|Q_A|^2 + |Q_B|^2]^2$$
$$+ v|Q_A Q_B|^2 + \sum_n \left[\frac{1}{2}(T-T_n)Q_n^2 + wQ_n^4\right], \quad \text{(A5)}$$

where Q_n is the real valued amplitude associated with the magnetic irrep Γ_n at zero wave vector and we have assumed a simplified form for the quartic interaction of zero wave vector irreps. Here, we assume that u and $u+v/4$ are strongly positive so that the transition near $T = T_q \approx 26$ K at which ICM order appears is definitely a continuous one. Also, T_n is the bare value of the temperature below which Q_n becomes nonzero. This free energy is equivalent to Eq. (1) of Ref. 7, although our interpretation of its consequences seems to be different from theirs.

By time reversal (T) symmetry, the free energy has no terms of odd order in Q_n. We assume continuous phase transitions, in which case, we consider the lowest-order interaction between CM and ICM order parameters, which is of the form

$$\Delta F = f(Q_n)[|Q_A|^2 + |Q_B|^2] + V(Q_n)[|Q_A|^2 - |Q_B|^2]. \quad \text{(A6)}$$

Since $|Q_A|^2 + |Q_B|^2$ is an invariant, the first term simply renormalizes the T_n, and we drop it. As we shall see, the second term represents a symmetry-breaking perturbation caused by the presence of ICM order. Since $|Q_A|^2 - |Q_B|^2$ is even under inversion but odd under 2_b, $V(Q_n)$ has to have this same symmetry. Then, using Table I, we see that the leading perturbation to the free energy is

$$\Delta F = aQ_1Q_3[|Q_A|^2 - |Q_B|^2] + bQ_2Q_4[|Q_A|^2 - |Q_B|^2]. \quad \text{(A7)}$$

The conclusion is this: if v in Eq. (A5) is negative so that the fourth-order ICM free energy favors $|Q_A|^2 = |Q_B|^2$, then we have a four q state, and the presence of ICM order does not lead to a symmetry-breaking term as in Eq. (A7). If $v > 0$, so that $Q_AQ_B = 0$, then we have a two-q state, and the perturbation of Eq. (A7) leads to a quadratic free energy for the zero wave-vector sector of Q_4 and Q_2 of the form

$$F = \tfrac{1}{2}[T - T_1]Q_1^2 + \tfrac{1}{2}[T - T_3]Q_3^2 + \lambda Q_1 Q_3, \quad \text{(A8)}$$

where $\lambda = a[|Q_A|^2 - |Q_B|^2]$. Since we expect λ to be small, this means that in the presence of this type of ICM order, the normal mode will consist mainly of Q_4 but with a small ($\sim|\lambda/(T_4 - T_2)|$) admixture of Q_2 and vice versa. The same statement can be made about Q_1 and Q_3 but with a different admixture coefficient λ'.

---

*Corresponding author: whli@phy.ncu.edu.tw

[1] S. A. Ivanov, R. Tellgren, C. Ritter, P. Nordblad, R. Mathieu, G. André, N. V. Golubko, E. D. Politova, and M. Weil, Mater. Res. Bull. **47**, 63 (2012).

[2] R. Becker, M. Johnsson, and H. Berger, Acta Crystallogr. Sec. C **62**, i67 (2006).

[3] M. Hudl, R. Mathieu, S. A. Ivanov, M. Weil, V. Carolus, Th. Lottermoser, M. Fiebig, Y. Tokunaga, Y. Taguchi, Y. Tokura, and P. Nordblad, Phys. Rev. B **84**, 180404(R) (2011).

[4] J. L. Her, C.-C. Chou, Y. H. Matsuda, K. Kindo, H. Berger, K. F. Tseng, C.-W. Wang, W.-H. Li, and H.-D. Yang, Phys. Rev. B **84**, 235123 (2011).

[5] W.-H. Li, C.-W. Wang, D. Hsu, C.-H. Lee, C.-M. Wu, C.-C. Chou, H.-D. Yang, Y. Zhao, S. Chang, J. W. Lynn, and H. Berger, Phys. Rev. B **85**, 094431 (2012).

[6] A. B. Harris, Phys. Rev. B **85**, 100403(R) (2012).

[7] P. Tolédano, V. Carolus, M. Hudl, T. Lottermoser, D. D. Khalyavin, S. A. Ivanov, and M. Fiebig, Phys. Rev. B **85**, 214439 (2012).

[8] T. Kimura, T. Goto, H. Shintani, K. Ishizaka, T. Arima, and Y. Tokura, Nature (London) **426**, 55 (2003).

[9] G. Lawes, A. B. Harris, T. Kimura, N. Rogado, R. J. Cava, A. Aharony, O. Entin-Wohlman, T. Yildirim, M. Kenzelmann, C. Broholm, and A. P. Ramirez, Phys. Rev. Lett. **95**, 087205 (2005).

[10] M. Kenzelmann, A. B. Harris, S. Jonas, C. Broholm, J. Schefer, S. B. Kim, C. L. Zhang, S.-W. Cheong, O. P. Vajk, and J. W. Lynn, Phys. Rev. Lett. **95**, 087206 (2005).

[11] G. R. Blake, L. C. Chapon, P. G. Radaelli, S. Park, N. Hur, S.-W. Cheong, and J. Rodríguez-Carvajal, Phys. Rev. B **71**, 214402 (2005).

[12] C. R. dela Cruz, F. Yen, B. Lorenz, M. M. Gospodinov, C. W. Chu, W. Ratcliff, J. W. Lynn, S. Park, and S.-W. Cheong, Phys. Rev. B **73**, 100406(R) (2006).

[13] A. Muñoz, M. T. Casáis, J. A. Alonso, M. J. Martínez-Lope, J. L. Martínez, and M. T. Fernández-Díaz, Inorg. Chem. **40**, 1020 (2001).

[14] S. A. Wolf, D. D. Awschalom, R. A. Buhrman, J. M. Daughton, S. von Molnár, M. L. Roukes, A. Y. Chtchelkanova, and D. M. Treger, Science **294**, 1488 (2001).

[15] *International Tables for Crystallography, Vol. A: Space-Group Symmetry*, 2nd ed., edited by T. Hahn (Kluwer Academic Publishers, Dordrecht, The Netherlands, 1993), p. 101.

[16] M. Fiebig, J. Phys. D **38**, R123 (2005).

[17] S. Skanthakumar, J. W. Lynn, J. L. Peng, and Z. Y. Li, Phys. Rev. B **47**, 6173 (1993).

[18] For a nonspecial wave vector, one might invoke two modes at the same wave vector. See A. Dixit, G. Lawes, and A. B. Harris, Phys. Rev. B **82**, 024430 (2010); B. Mettout and P. Tolédano, J. Phys.: Condens. Matter **24**, 086002 (2012).

[19] A. C. Larson and R. B. von Dreele, General Structure Analysis System Report, LAUR 86-748 (Los Alamos National Laboratory, Los Alamos, NM, 2004).

[20] T. Kimura, G. Lawes, T. Goto, Y. Tokura, and A. P. Ramirez, Phys. Rev. B **71**, 224425 (2005).

[21] J. Baier, D. Meier, K. Berggold, J. Hemberger, A. Balbashov, J. A. Mydosh, and T. Lorenz, Phys. Rev. B **73**, 100402(R) (2006)

[22] J. Rodríguez-Carvajal, Physica B **192**, 55 (1993).

[23] T. Horiguchi, Phys. Lett. A **113**, 425 (1986).

[24] J. B. Fouet, P. Sindzingre, and C. Lhuiller, Eur. Phys. J. B **20**, 241 (2001).

[25] W. L. Roth, Phy. Rev. **110**, 1333 (1958).

[26] W. L. Roth, J. Phys. Chem. Solids **25**, 1 (1964).

[27] A. Sazonov, V. Hutanu, M. Meven, G. Heger, A. Gukasov, and A. Rogalev, J. Phys.: Conf. Ser. **211**, 012011 (2010).

[28] M. Maglione, U. T. Höchli, J. Joffrin, and K. Knorr, J. Phys.: Condens. Matter **1**, 1527 (1989).

[29] W. A. Kamitakahara, C.-K. Loong, G. E. Ostrowski, and L. A. Boatner, Phys. Rev. B **35**, 223 (1987).

[30] D. La-Orauttapong, J. Toulouse, Z.-G. Ye, W. Chen, R. Erwin, and J. L. Robertson, Phys. Rev. B **67**, 134110 (2003).

[31] K. C. Rule, M. Reehuis, M. C. R. Gibson, B. Ouladdiaf, M. J. Gutmann, J.-U. Hoffmann, S. Gerischer, D. A. Tennant, S. Süllow, and M. Lang, Phys. Rev. B **83**, 104401 (2011).

[32] T. Kimura, Annu. Rev. Mater. Res. **37**, 387 (2007).

[33] Y. Tokura and S. Seki, Adv. Mater. **22**, 1554 (2010).

[34] H. Katsura, N. Nagaosa, and A. V. Balatsky, Phys. Rev. Lett. **95**, 057205 (2005).

[35] I. Cabrera, M. Kenzelmann, G. Lawes, Y. Chen, W. C. Chen, R. Erwin, T. R. Gentile, J. B. Leão, J. W. Lynn, N. Rogado, R. J. Cava, and C. Broholm, Phys. Rev. Lett. **103**, 087201 (2009).

[36] S. Seki, Y. Yamasaki, M. Soda, M. Matsuura, K. Hirota, and Y. Tokura, Phys. Rev. Lett. **100**, 127201 (2008).

[37] Y. Yamasaki, H. Sagayama, T. Goto, M. Matsuura, K. Hirota, T. Arima, and Y. Tokura, Phys. Rev. Lett. **98**, 147204 (2007).

[38] H. Singh *et al.*, arXiv:1309.6417.